Acute *Trem2* reduction triggers increased microglial phagocytosis, slowing amyloid deposition in mice

Kathleen M. Schoch[a,1], Lubov A. Ezerskiy[a], Michaela M. Morhaus[a], Riley N. Bannon[a], Andrew D. Sauerbeck[a], Mark Shabsovich[a], Paymaan Jafar-nejad[b], Frank Rigo[b], and Timothy M. Miller[a,1]

[a]Department of Neurology, Hope Center for Neurological Disorders, Washington University in St. Louis, St. Louis, MO 63110; and [b]Ionis Pharmaceuticals, Carlsbad, CA 92010

Edited by Hugo Bellen, Baylor College of Medicine, Houston, TX, and approved May 25, 2021 (received for review January 12, 2021)

Heterozygous genetic variants within the *TREM2* gene show a strong association with increased Alzheimer's disease (AD) risk. Amyloid beta–depositing mouse models haploinsufficient or null for *Trem2* have identified important relationships among TREM2, microglia, and AD pathology; however, results are challenging to interpret in the context of varying microglial phenotypes and disease progression. We hypothesized that acute *Trem2* reduction may alter amyloid pathology and microglial responses independent of genetic *Trem2* deletion in mouse models. We developed antisense oligonucleotides (ASOs) that potently but transiently lower *Trem2* messenger RNA throughout the brain and administered them to APP/PS1 mice at varying stages of plaque pathology. Late-stage ASO-mediated *Trem2* knockdown significantly reduced plaque deposition and attenuated microglial association around plaque deposits when evaluated 1 mo after ASO injection. Changes in microglial gene signatures 1 wk after ASO administration and phagocytosis measured in ASO-treated cells together indicate that microglia may be activated with short-term *Trem2* reduction. These results suggest a time- and/or dose-dependent role for TREM2 in mediating plaque deposition and microglial responses in which loss of TREM2 function may be beneficial for microglial activation and plaque removal in an acute context.

Alzheimer's disease | amyloid | antisense oligonucleotide | microglia | Trem2

A defining feature of Alzheimer's disease (AD) is the abnormal deposition of amyloid beta (Aβ) plaques within the brain, appearing in cognitively normal individuals before the onset of clinical symptoms (1). As one of the earliest pathological events identified in AD (2), Aβ accumulation may be an upstream trigger for additional pathological hallmarks including tau accumulation, synaptic dysfunction, and neurodegeneration. Plaque pathology is also associated with neuroinflammatory responses that acutely may serve a protective function but with chronic activation may contribute to cell death (3–5). Genome wide association studies further underscore the importance of the immune response in modulating the development or progression of AD with several immune-related genes showing significant associations with AD risk (6). Among these, variants identified within the gene *TREM2* (triggering receptor expressed on myeloid cells 2) were found to confer an ~threefold increased risk for late onset AD (7, 8), thus generating considerable interest in understanding how TREM2 modulates neuroinflammation and AD pathogenesis.

TREM2 is a membrane-associated receptor found on microglia in the central nervous system (CNS) as well as peripheral macrophages and dendritic cells (9). In vitro studies suggest that, upon activation by extracellular ligands, TREM2 mediates intracellular signaling cascades to repress inflammatory cytokine production or secretion and to increase phagocytosis (10). However, the role of TREM2 in disease is less clear and likely complicated by the changing neuroinflammatory and neurodegenerative environment. In AD, microglial gene signatures shift from a homeostatic to neurodegenerative state (11, 12), with *TREM2* up-regulation serving as a critical checkpoint in this progression (12). In addition, perturbations in TREM2 expression consistently reduce microglial clustering around Aβ plaques (13–17), suggesting TREM2 facilitates an interaction between microglia and plaque pathology. Together, these data highlight a role for TREM2 in directing microglial responses in disease and controlling the ability of microglia to surround, contain, or clear Aβ.

The dual role of TREM2 in mediating immune cell responses as well as plaque pathology makes TREM2 an attractive therapeutic target, yet it is not clear whether or in what contexts TREM2 is acting to perpetuate microglial activity and toxic neuroinflammation or to protect the brain from amyloid spread and inflammatory damage. Several studies have investigated *Trem2*$^{-/-}$ in amyloid-depositing mouse models to determine the effect of TREM2 loss on microglial function and AD pathology. Absence of *Trem2* has been shown to alter plaque morphology (16), increase plaque deposition (13, 15), promote neuritic dystrophy (16, 18), and facilitate phosphorylated tau seeding (19), supporting the conclusion that TREM2-mediated microglial responses exert a protective role in AD. However, TREM2 function and microglial activation also may depend on other factors, such as age (20–22), disease insult or injury (23–25), gene dosage (26), and the presence of Aβ and/or tau pathology (19, 27–29), which together reveal specific contexts

Significance

Alzheimer's disease (AD) remains a significant health burden within the aging population and currently lacks therapies that effectively target pathological events to halt the development or progression of AD. The gene *TREM2* appears to influence abnormal protein accumulations in AD through the brain's immune cells; however, it is not clear if and when TREM2 might be targeted in disease to limit pathology or the immune response. We used antisense oligonucleotides (ASOs) to reduce *Trem2* levels in the mouse brain at specific times in disease and investigated amyloid protein accumulations, microglial responses, and genetic signatures. ASO-mediated *Trem2* lowering during late-stage disease reduced amyloid pathology, which may have been triggered by an acute activation of microglia to engulf and clear amyloid deposits.

Author contributions: K.M.S., P.J.-n., F.R., and T.M.M. designed research; K.M.S., L.A.E., M.M.M., and R.N.B. performed research; P.J.-n. and F.R. contributed new reagents/analytic tools; K.M.S., L.A.E., M.M.M., R.N.B., A.D.S., M.S., and T.M.M. analyzed data; K.M.S. and T.M.M. wrote the paper; and L.A.E., M.M.M., R.N.B., A.D.S., M.S., P.J.-n., T.M.M., and F.R. reviewed the paper.

Competing interest statement: P.J.-N. and F.R. are paid employees of Ionis Pharmaceuticals. Washington University in St. Louis has an existing licensing agreement with Ionis Pharmaceuticals for use of antisense oligonucleotides in these studies. T.M.M. is a consultant for Ionis Pharmaceuticals.

This article is a PNAS Direct Submission.

[1]To whom correspondence may be addressed. Email: miller.t@wustl.edu or kmschoch@wustl.edu.

This article contains supporting information online at https://www.pnas.org/lookup/suppl/doi:10.1073/pnas.2100356118/-/DCSupplemental.

Published June 29, 2021.

in which TREM2 may have distinct functions, both beneficial and detrimental, within disease. While genetic *Trem2*$^{-/-}$ mouse models clearly support a role for TREM2 function in Aβ pathology and microglia-mediated neurodegeneration, these models are limited in their ability to inform on TREM2 involvement in distinct disease mechanisms, such as deposition versus degradation of amyloid. Therefore, it is unclear which therapeutic strategies—aimed at increasing or decreasing TREM2 levels—may be beneficial to disease.

In this study, we investigated how acute *Trem2* reduction in an adult animal influences Aβ pathology and microglial function to inform upon TREM2-targeted interventions. We designed antisense oligonucleotides (ASOs) to achieve specific lowering of *Trem2* messenger RNA (mRNA) in the Aβ-depositing APP/PS1 mouse model before, during, and after the onset of pathology. We show that ASO-mediated *Trem2* reduction in vivo is effective and widespread following a single CNS injection. Lowering *Trem2* afforded a robust reduction of existing amyloid deposition when administered during late-stage Aβ pathology but was not effective if given prior to or at an early stage of plaque pathology. Despite a decrease in plaque-associated microglia and select canonical activation signals 1 mo after *Trem2* reduction, gene expression patterns suggested increased activation and elevated phagocytic responses with acute ASO treatment. The results presented here support a benefit for temporary TREM2 reduction during the later stages of amyloid pathology and may help clarify the potential consequences of TREM2-targeting therapies in AD patients.

Results

ASOs Effectively Reduce Trem2 Levels in APP/PS1 Mice. We developed *Trem2*-targeted ASOs designed for *Trem2* mRNA degradation and characterized ASO efficacy, duration, and distribution in vivo. APP/PS1 mice at 10 mo of age were treated with a single intracerebroventricular (ICV) injection of inactive ASO or *Trem2* knockdown (KD) ASO. At this age, APP/PS1 mice exhibit robust amyloid pathology and gliosis corresponding to late-stage disease (30–32). *Trem2* mRNA was significantly elevated in inactive ASO-treated APP/PS1 mice compared with nontransgenic controls (Fig. 1*A*), consistent with increased TREM2 expression in other amyloid-depositing mouse models (13, 33, 34) and human AD (35–37). Elevated *Trem2* mRNA levels were also evident in brain tissue from untreated 10-mo-old APP/PS1 mice, verifying the inactive ASO did not significantly alter *Trem2* levels (Fig. 1*A*). Treatment with *Trem2* KD ASO substantially decreased *Trem2* mRNA levels in frontal, parietal, occipital, and cerebellum regions (Fig. 1*A*), confirming both the widespread distribution and overall effectiveness of the *Trem2* KD ASO. In addition, *Trem2* reduction from a single injection was persistent, showing significantly less *Trem2* mRNA levels compared with controls 8 wk past the initial injection but returning to control levels by 16 wk postinjection (*SI Appendix*, Fig. S1*A*). The reduction of *Trem2* mRNA was coincident with reduced TREM2 protein reactivity identified via immunohistochemical staining of brain sections from treated APP/PS1 mice (Fig. 1 *B* and *C* and *SI Appendix*, Fig. S2). Collectively, these data show effective, sustained, and widespread reduction of TREM2 after a single ICV injection.

Trem2 mRNA levels in peripheral tissues of treated APP/PS1 mice showed no significant differences between treatments, confirming the CNS-specific effect of *Trem2*-targeted ASOs (*SI Appendix*, Fig. S1*B*). To investigate possible off-target effects, we evaluated mRNA levels of genes whose gene or transcript sequences were most similar to the *Trem2* ASO sequence and found no significant changes across ASO treatment (*SI Appendix*, Fig. S1*C*). A 75% sequence alignment was identified between the *Trem2* KD ASO and *Runx1*, a gene implicated in microglial activation states; however, downstream transcription factor expression of *SPI1* remained unchanged, and we excluded *Runx1* as a sequence-dependent off-target gene. Given the effectiveness and specificity of the *Trem2*-targeted ASO in vivo, subsequent experiments used the same single ASO injection paradigm to investigate the pathological effects of *Trem2* lowering in APP/PS1 mice.

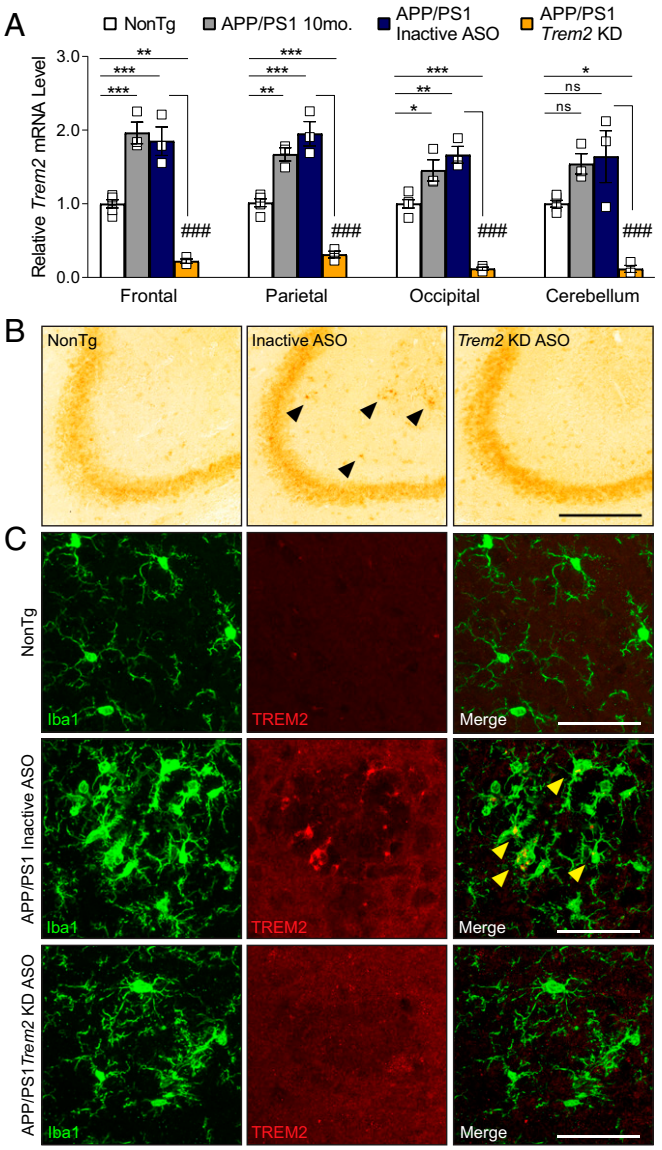

Fig. 1. ASOs reduce TREM2 throughout the brain of APP/PS1 mice. (*A*) Brain tissue from 11-mo-old APP/PS1 and nontransgenic (NonTg, $n = 5$) mice was analyzed for *Trem2* mRNA by qRT-PCR 1 mo following intracerebroventricular injection of inactive ASO or *Trem2* KD ASO ($n = 3$/group). Tissues from untreated APP/PS1 mice at 10 mo of age ($n = 3$) were included as a control. mRNA was normalized to *GAPDH* and expressed as mean ± SEM; one-way ANOVA with Tukey's multiple comparison test; $^{*}P < 0.05$, $^{**}P < 0.01$, $^{***}P < 0.001$ versus NonTg; $^{\#\#\#}P < 0.001$ versus APP/PS1 10 mo and inactive ASO; ns, nonsignificant. Individual mice are depicted as open squares. (*B*) Representative images of Trem2 immunohistochemistry from brain tissue contralateral to the ASO injection from NonTg and ASO-treated APP/PS1 mice. The CA3 regions of the hippocampus are shown, with arrowheads indicating TREM2-positive areas. (Scale bar, 250 μm.) (*C*) Representative images of Iba1 (green) and TREM2 (red) immunofluorescence within the retrosplenial cortex are shown, with arrowheads indicating colocalized (yellow) regions. (Scale bar, 50 μm.)

Lowering Trem2 in APP/PS1 Mice Reverses Late-Stage Amyloid Beta Deposition. Increased TREM2 expression identified in amyloid-depositing mouse models and human AD is associated with plaque deposits (13, 34), and Aβ has been identified as a ligand for the

TREM2 receptor (38). In addition, mice with *Trem2* deficiency from birth exhibit changes to plaque morphology and number (15, 16), suggesting that perturbation of a TREM2–amyloid interaction may influence plaque deposition or pathogenicity; however, this effect may depend on the stage of disease (20). To better inform on the effect of an acute *Trem2*-targeted intervention on plaque load, APP/PS1 mice were given a single ICV injection of inactive or *Trem2* KD ASO at 4, 7, or 10 mo of age to parallel preplaque, early plaque, and postplaque stages of disease. *Trem2* mRNA levels (*SI Appendix*, Fig. S3) and Aβ deposition (Fig. 2 and *SI Appendix*, Fig. S4) were analyzed at 11 mo of age. Consistent with the duration of action of *Trem2*-targeted ASOs in our initial characterization (*SI Appendix*, Fig. S1*A*), *Trem2* mRNA levels were significantly decreased at 1 mo post-ASO injection but had returned to control levels 4 and 7 mo postinjection (*SI Appendix*, Fig. S3). APP/PS1 mice treated with inactive ASO exhibited extensive amyloid deposition throughout the cortex and hippocampus (Fig. 2*A*). Strikingly, a robust, significant decrease in plaque deposition was identified in APP/PS1 mouse brains 1 mo following *Trem2* KD ASO injection at 10 mo of age compared with inactive ASO-treated mice (Fig. 2 *B* and *C*). Furthermore, *Trem2* lowering appears to eliminate plaques present at the time of injection, as the area of Aβ following *Trem2* KD ASO treatment was significantly less than untreated 10-mo-old APP/PS1 mice (Fig. 2*C*). Fibrillar plaques, identified by X-34 staining, were also significantly reduced in both the cortex and hippocampus after *Trem2* KD ASO treatment (Fig. 2 *D*–*F*). *Trem2* lowering at 4 and 7 mo of age did not significantly affect plaque load when assessed later in disease (*SI Appendix*, Fig. S4). These data suggest acutely lowering *Trem2* mRNA in adult mice after plaque deposition can promote plaque clearance to reverse existing plaque pathology.

Trem2 Reduction in APP/PS1 Mice Attenuates Phosphorylated tau Levels. Although endogenous mouse tau is not expected to form AD-like tau tangles, amyloid-depositing mice exhibit measurable levels of phosphorylated tau (39–41) that may be a secondary effect of amyloid beta pathology; therefore, we immunostained for phosphorylated tau using the antibody AT8 in brain tissue from inactive- and *Trem2*-lowering ASO-treated APP/PS1 mice and their nontransgenic littermate controls. At 11 mo of age (1 mo past ASO injection), elevated AT8 reactivity was detectable in the cortex and hippocampus of APP/PS1 mice treated with the inactive ASO (Fig. 3 *A* and *C*) compared with nontransgenic controls and appeared similar in localization to amyloid plaque staining, perhaps indicative of phosphorylated tau in dystrophic neurites. With ASO-mediated *Trem2* KD, however, AT8 staining appeared to decrease (Fig. 3 *B* and *D*), and both the area of AT8 staining (Fig. 3*E*) and number of AT8 puncta (Fig. 3*F*) within the cortex and hippocampus were significantly reduced with *Trem2*-lowering ASO treatment compared with inactive ASO controls. These results are consistent with less plaque pathology after *Trem2* reduction, suggesting decreased amyloid load or neuroinflammation may attenuate downstream tau phosphorylation.

Plaque-Associated Microglia Decrease with Trem2-Lowering ASO Treatment. Genetic loss of *Trem2* in Aβ-depositing mice reduces microglial clustering around amyloid plaques (13–17), which may permit an increase in plaque load or pathogenesis (18, 42). However, we observed a robust reduction in plaque deposition after ASO-mediated *Trem2* lowering. To understand how acute *Trem2* KD ASO treatment may have altered microglia, particularly plaque-associated microglia, brain tissue from ASO-treated APP/PS1 mice was analyzed for the microglial marker Iba1 in association with amyloid plaques 1 mo following ASO injection

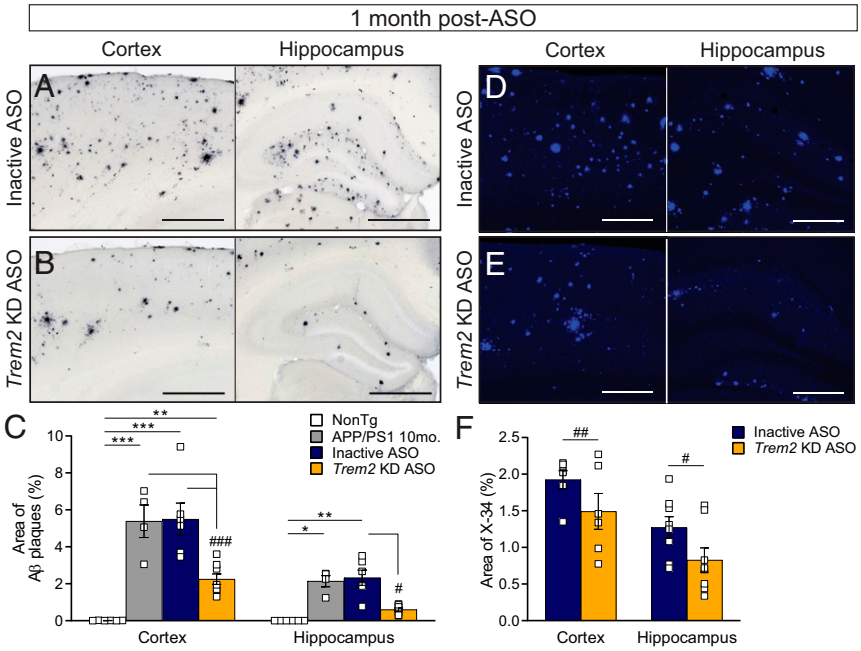

Fig. 2. *Trem2*-lowering ASO treatment reverses amyloid deposition during late stages of plaque development. Cortical and hippocampal regions from 11-mo-old nontransgenic (NonTg) and APP/PS1 mice were analyzed for amyloid beta (Aβ) deposition (antibody: HJ3.4) 1 mo following treatment with (*A*) inactive or (*B*) *Trem2* KD ASO. Representative images are shown. (Scale bar, 500 μm.) (*C*) The area of Aβ plaques was quantified within the cortex and hippocampus of ASO-treated mice. Untreated APP/PS1 mice at 10 mo of age were included for comparison. Data are mean ± SEM. Open squares represent individual mice: $n = 6$ NonTg, $n = 4$ 10-mo APP/PS1, $n = 6$ inactive ASO, and $n = 8$ *Trem2* KD ASO. One-way ANOVA with Tukey's multiple comparison test; $^{*}P < 0.05$, $^{**}P < 0.01$, and $^{***}P < 0.001$ versus NonTg; $^{\#}P < 0.05$ and $^{\#\#\#}P < 0.001$ versus untreated or inactive ASO. Brains were similarly analyzed for Aβ deposition by X-34 staining following (*D*) inactive or (*E*) *Trem2* KD ASO treatment. Representative images are shown. (Scale bar, 250 μm.) (*F*) The area of X-34 staining was quantified within the cortex and hippocampus of ASO-treated mice. Data are mean ± SEM. Open squares represent individual mice: $n = 6$ inactive ASO and $n = 8$ *Trem2* KD ASO. Unpaired *t* test; $^{\#}P < 0.05$, $^{\#\#}P < 0.01$ versus inactive ASO.

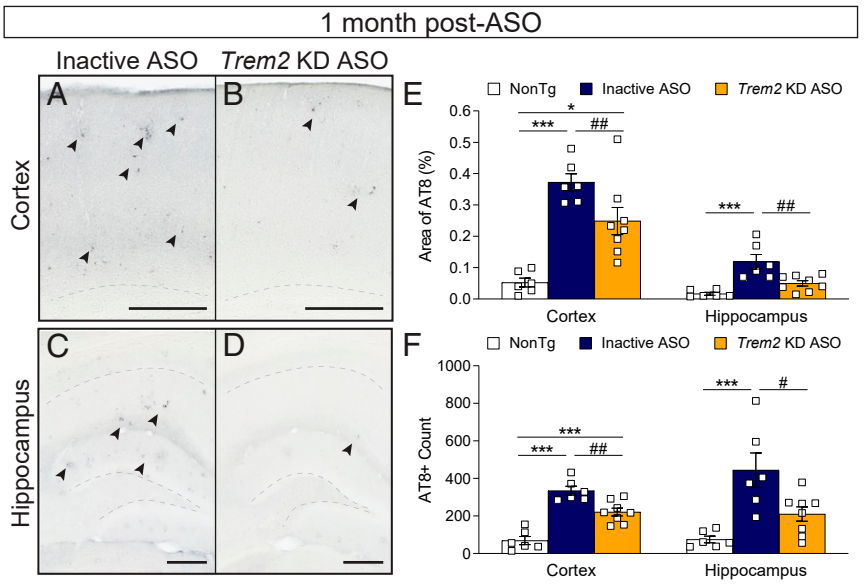

Fig. 3. Phosphorylated tau levels are reduced following *Trem2* reduction. Brain tissue from 11-mo-old nontransgenic (NonTg) and APP/PS1 mice were immunostained for phosphorylated tau (antibody: AT8) 1 mo following treatment with inactive or *Trem2* KD ASO. Representative images from the (*A* and *B*) cortex and (*C* and *D*) hippocampus are shown. (Scale bar, 250 μm.) Arrows indicate regions of AT8 positivity. Dotted lines denote the subcortical white matter in *A* and *B* and the CA1 and dentate gyrus layers in *C* and *D*. (*E*) The area of AT8 reactivity and (*F*) number of AT8 puncta were quantified within the cortex and hippocampus. Data are mean ± SEM; one-way ANOVA with Tukey's multiple comparison test. $^{*}P < 0.05$, $^{***}P < 0.001$ versus NonTg; $^{\#}P < 0.05$, $^{\#\#}P < 0.01$ versus inactive ASO. Open squares represent individual mice: $n = 6$ NonTg, $n = 6$ inactive ASO, and $n = 8$ *Trem2* KD ASO.

given at 10 mo of age. APP/PS1 mice treated with inactive ASO exhibited robust Iba1 reactivity, with microglia concentrated around HJ3.4-positive amyloid plaques and appearing with large somas and retracted processes (Fig. 4*A*). In comparison, microglia surrounding plaques in tissue from APP/PS1 mice treated with *Trem2* KD ASO appeared less reactive, displaying small somas and long processes (Fig. 4*B*). When quantified within the hippocampus, Iba1 coverage per plaques was significantly lessened with *Trem2* KD compared with inactive ASO treatment (Fig. 4*C* and *SI Appendix*, Fig. S5*A*), yet the total number of microglia was not significantly altered across groups (Fig. 4*D*).

In addition to clustering around plaques, microglia can also exert inflammatory functions especially in response to amyloid accumulation and aging (43). Therefore, we sought to evaluate the inflammatory state of the brain 1 mo following *Trem2* reduction in 10-mo-old APP/PS1 mice. Whole-brain tissue homogenates from ASO-treated APP/PS1 mice were analyzed for inflammatory-related genes, microglial markers, and components of the complement pathway (Fig. 4*E* and *SI Appendix*, Fig. S6*A*). *Tyrobp* (encodes DAP12 coreceptor for TREM2) and *IL1-β* levels were significantly increased in APP/PS1 mice treated with inactive ASO compared with nontransgenic but were dampened after *Trem2* KD ASO treatment (Fig. 4*E*). Similarly, APP/PS1 mice treated with inactive ASO displayed a significant up-regulation of *CD68* and *Cst7* (cystatin F), genes indicative of microglial activation/phagocytosis; however, *Trem2* KD ASO administration suppressed *CD68* levels to nontransgenic levels and *Cst7* levels by over half compared with control treatment (Fig. 4*E*). GFAP levels were also increased in APP/PS1 mice but reduced with *Trem2* KD ASO treatment; however, transcript levels of the remaining genes tested were not significantly changed with genotype or ASO treatment (*SI Appendix*, Fig. S6*A*). Together, these transcriptional changes suggest modulation of the TREM2–DAP12 signaling pathway toward dampened inflammation and less microglial activation with ASO-mediated *Trem2* lowering.

Acute Trem2 Reduction Spurs Microglial Activation. Plaque-associated microglia and microglial gene expression data measured 1 mo following ASO treatment suggest that *Trem2* lowering suppresses microglial activity, consistent with studies in *Trem2*$^{-/-}$ mouse models. However, a reduced microglial response does not explain the reduction of amyloid plaque deposition in the brains of *Trem2* KD ASO-treated APP/PS1 mice. To interrogate acute microglial responses prior to plaque removal, we treated 10-mo-old APP/PS1 mice with inactive or *Trem2*-lowering ASO and analyzed brain tissue 1 wk later. At this time point, *Trem2* mRNA levels were significantly lowered with *Trem2* KD ASO treatment compared with nontransgenic and ASO controls (*SI Appendix*, Fig. S3*D*). Plaque deposition in the cortex and hippocampus was unchanged by ASO treatment (Fig. 5 *A*–*C*). Microglial coverage around plaques (Fig. 5 *D*–*F* and *SI Appendix*, Fig. S5*B*) and total microglial numbers (Fig. 5*G*) within the hippocampus were also similar across groups. Markers of inflammatory and microglial genes, however, suggested a pattern of increased activation. Levels of *Cst7* were significantly elevated in APP/PS1 mice regardless of ASO treatment, suggesting a general up-regulation of inflammation due to amyloid pathology (Fig. 5*H*). Levels of *Iba1* and *Apoe* were significantly increased in mice treated with *Trem2* KD ASO compared with control mice (Fig. 5*H* and *SI Appendix*, Fig. S6*B*), consistent with activation of a microglial-specific genetic signature. *Hexb*, a gene associated with homeostatic microglia, was also up-regulated with *Trem2*-lowering treatment compared with controls (*SI Appendix*, Fig. S6*B*). Together, these results suggest microglia may be acutely activated to promote phagocytosis and clear amyloid plaques over time. Therefore, we investigated phagocytic activity of cultured cells following ASO-mediated *Trem2* reduction (Fig. 6 and *SI Appendix*, Fig. S7). BV2 cells treated with *Trem2* KD ASO showed a significant increase in their ability to engulf fluorescently labeled beads compared with inactive ASO treatment (Fig. 6 *A*–*C*). Similarly, primary microglia from nontransgenic mice treated with *Trem2*-lowering ASO exhibited an increase in phagocytic activity versus control-treated cells (Fig. 6 *D*–*F*).

Discussion

We developed *Trem2*-lowering ASOs that specifically and effectively reduce *Trem2* levels throughout the adult mouse CNS. Acute *Trem2* reduction in the presence of late-stage plaque pathology

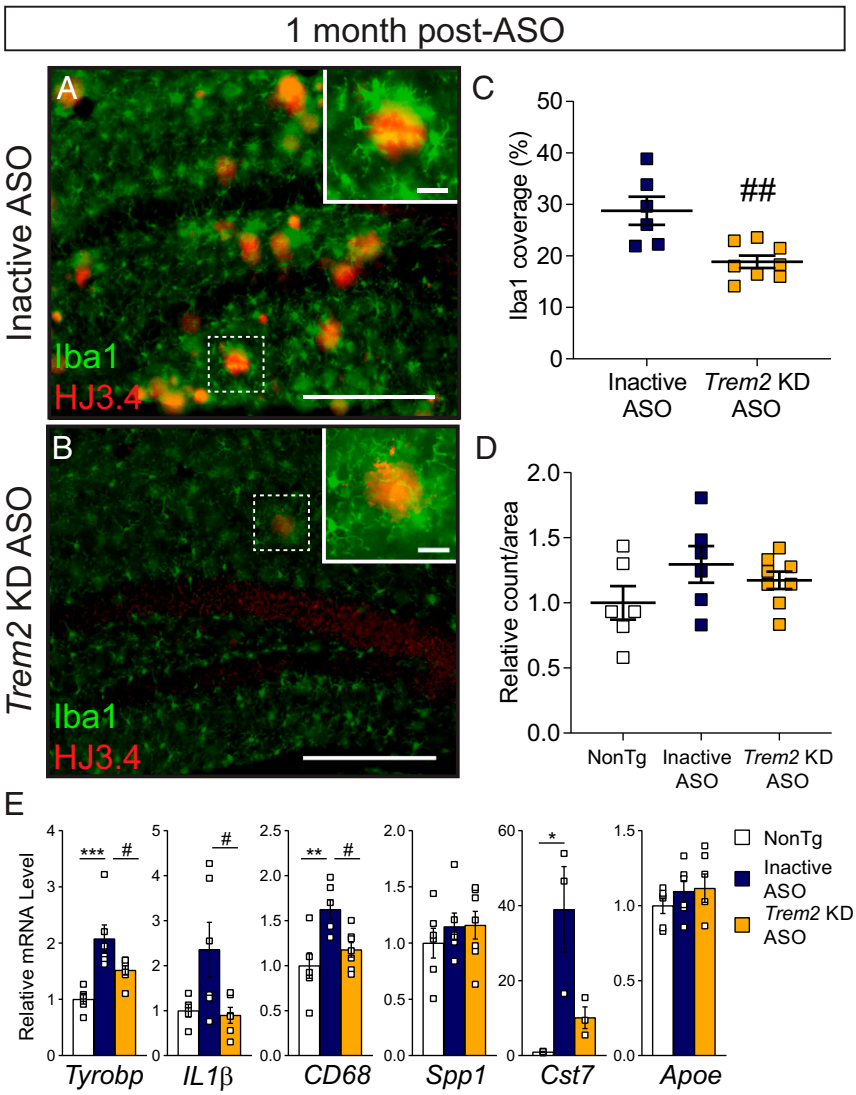

Fig. 4. Microglial localization and genetic responses are blunted 1 mo following late-stage *Trem2* reduction. Brain tissue from 11-mo-old APP/PS1 mice treated with (*A*) inactive or (*B*) *Trem2* KD ASO 1 mo prior was labeled with Iba1 to identify microglia (green) and HJ3.4 to identify amyloid beta plaques (red). Representative images are shown. (Scale bar, 250 μm, inset 25 μm.) (*C*) The area of Iba1+ coverage of plaques per animal and (*D*) total Iba1+ counts were quantified within the hippocampus following inactive ASO ($n = 6$) or *Trem2* KD ASO ($n = 8$) treatment. Nontransgenic (NonTg) mice ($n = 6$) included for total microglia quantification. Data are mean ± SEM; unpaired *t* test or one-way ANOVA; $^{\#\#}P < 0.01$. (*E*) mRNA levels of select inflammatory or microglial markers were measured by qRT-PCR and normalized to *GAPDH* (open square represent individual mice; $n = 3$ to 7/treatment). Data are mean ± SEM relative to NonTg; one-way ANOVA with Tukey's multiple comparison test; $^{*}P < 0.05$, $^{**}P < 0.01$, $^{***}P < 0.001$ versus NonTg; $^{\#}P < 0.05$ versus inactive ASO.

surprisingly suppressed plaque deposition and cleared existing plaque deposits, a result that was not achieved if *Trem2* lowering was initiated before or during plaque accumulation. Although microglial clustering around plaques was also lessened with *Trem2* reduction 1 mo after ASO injection, this effect may be secondary to a transient increase in microglial activation and phagocytic activity as was evident in acute in vivo and in vitro studies. By investigating a short-term *Trem2*-lowering paradigm in adult amyloid-depositing mice, this study supports a time- and/or duration-dependent role for TREM2 in mediating microglial responses to plaque pathology. We acknowledge that reducing TREM2 expression is somewhat counterintuitive given previous research supporting a loss-of-function mechanism for genetic TREM2 variants and increased AD risk. Furthermore, recent studies investigating the therapeutic potential of TREM2 agonists have found increased TREM2 function or expression reduces amyloid plaque load and supports protective microglial responses (44, 45). Our findings, however, suggest that acute, CNS-specific *Trem2* reduction may be beneficial toward lowering plaques and mitigating inflammatory responses. While both a *Trem2*-lowering ASO and TREM2 agonist represent a postpathology intervention in the absence of TREM2 mutation, the dichotomous results introduce a level of caution for therapies seeking to modulate levels of TREM2 in neurodegenerative diseases.

Trem2 deletion in mouse models expressing familial AD mutations have shown varying results particularly regarding plaque load, complicating interpretation of TREM2's function on microglia and Aβ pathology. While *Trem2*-deficient mouse models are important for understanding how genetic changes in TREM2 from birth due to rare variants may contribute to AD risk, they are less informative regarding the effect of changing TREM2 expression or activity in the adult, throughout the disease, or in sporadic AD. In the current study, acute *Trem2* lowering by ASO was achieved before, during, and after plaques deposit; however, only *Trem2* reduction after overt plaque accumulation was able to lessen plaque load overall. These findings suggest that TREM2 may have separate roles in

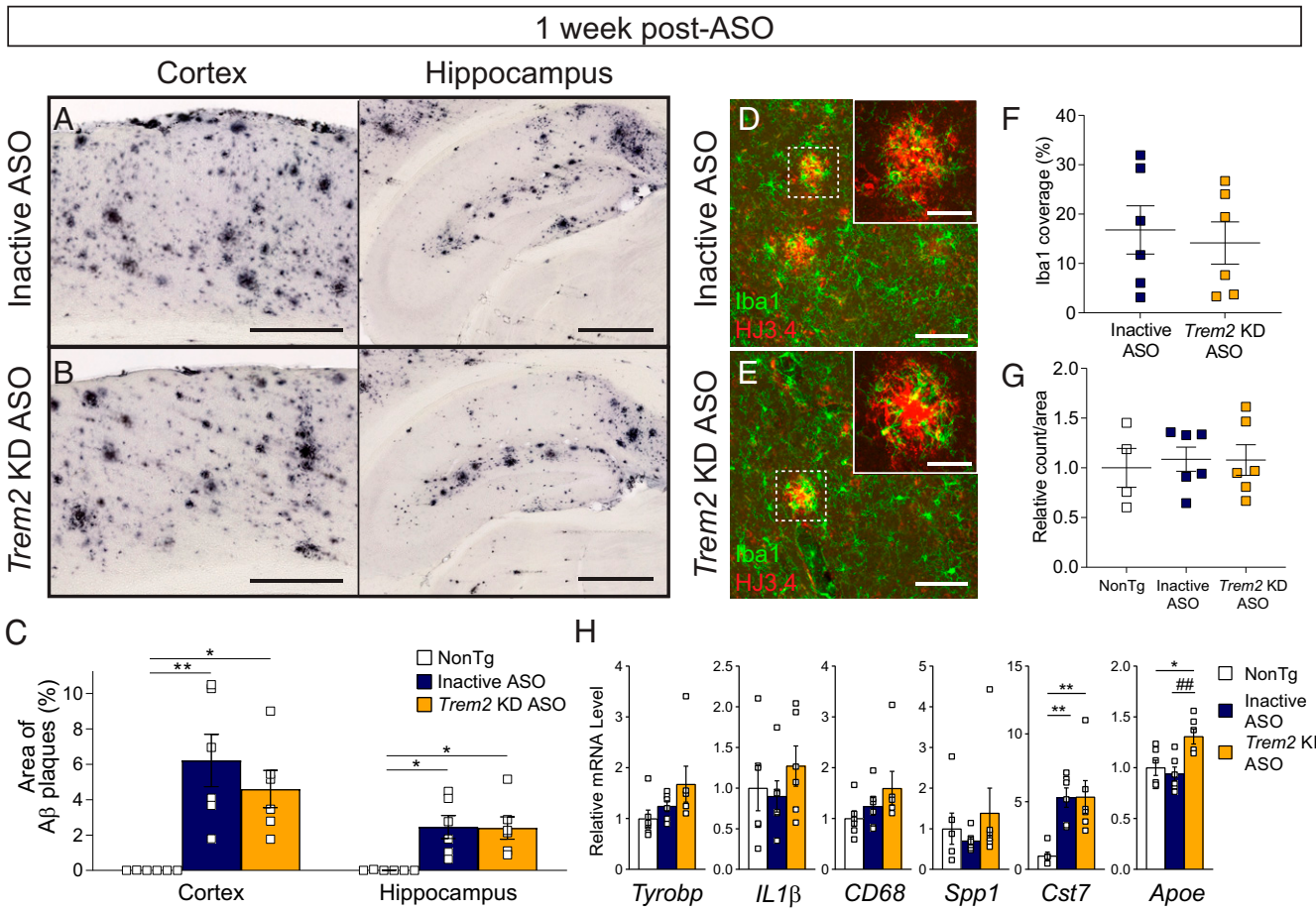

Fig. 5. Select activation markers are up-regulated 1 wk following late-stage *Trem2* reduction despite no change in amyloid deposition or microglial clustering. Nontransgenic (NonTg) and APP/PS1 mice were treated with (*A*) inactive or (*B*) *Trem2* KD ASO at 10 mo of age. One week after ASO injection, mice were euthanized and brain tissue labeled with HJ3.4 to identify amyloid beta plaques. Representative images are shown. (Scale bar, 500 μm.) (*C*) Amyloid deposition was quantified within the cortex and hippocampus and expressed as a percentage of the total area measured. Data are mean ± SEM; one-way ANOVA with Tukey's multiple comparison test; $^{*}P < 0.05$, $^{**}P < 0.01$ versus NonTg. Squares are individual mice ($n = 6$ per genotype/treatment). Brain tissue from mice treated with (*D*) inactive or (*E*) *Trem2* KD ASO were also immunofluorescently labeled with HJ3.4 (red) and Iba1 (green). Representative images are shown. (Scale bars, 100 μm, 25 μm for insets.) (*F*) The area of Iba1+ coverage of plaques per animal and (*G*) total Iba1+ counts were quantified within the hippocampus following inactive ASO ($n = 6$) or *Trem2* KD ASO ($n = 6$) treatment. Data are mean ± SEM. (*H*) mRNA levels of select inflammatory or microglial markers were measured by qRT-PCR, normalized to *GAPDH* (open square represent individual mice; $n = 3$ to 7/treatment). Data are mean ± SEM relative to NonTg; one-way ANOVA with Tukey's multiple comparison test; $^{*}P < 0.05$ and $^{**}P < 0.01$ versus NonTg; $^{\#\#}P < 0.01$ versus inactive ASO.

early-stage plaque deposition and postonset plaque clearance to potentially reactivate beneficial microglial responses or suppress aberrant ones. In support of a time-dependent role for TREM2 in AD, amyloid-depositing mice lacking *Trem2* exhibited decreased plaque load early in plaque development yet greater plaque burden later in disease compared with age-matched wild-type mice (20, 22). Although we and others (42) have observed the opposite effect in different transgenic models (i.e., decreased plaque load with *Trem2* reduction later in disease), the APP/PS1 mice used in our present studies develop plaques at a slower rate than the models used previously and, therefore, may exhibit altered pathological and microglial responses to *Trem2* loss. Our data suggest that *Trem2* lowering not only prevented plaque deposition but also promoted plaque clearance, possibly through the earlier activation of microglial genes to initiate phagocytosis. *Trem2* and additional microglial genetic signatures undergo temporal changes with age and disease progression that control microglial functions (11, 12, 46). We noted transient increases in *Iba1*, *Cst7*, and *Apoe* that were absent 1 mo after ASO injection, suggesting activation signals that may spur microglia into an activated state after *Trem2* reduction. Therefore, acute *Trem2* intervention with an ASO may revert microglia from a damage-associated state to instead limit plaque deposition by elevating phagocytic abilities or promoting an anti-inflammatory environment.

In our experiments, ASO-mediated *Trem2* lowering achieved a near complete reduction of *Trem2* mRNA levels at 1 mo postinjection, an effect that would be expected to last up to 2 mo using the current treatment paradigm. This transient TREM2 intervention may be responsible for the reversal of plaque pathology in parallel with reduced microglial clustering 1 mo later, revealing a dose- or duration-dependent function for TREM2 in AD. Heterozygous *TREM2* genetic risk variants identified in AD are predicted to afford a partial loss of function through altered protein stability (47, 48) or ligand binding (49), whereas homozygous *TREM2* mutations that result in Nasu-Hakola disease interfere with TREM2 cell-surface expression (48). Therefore, the level of remaining TREM2 expression or function may be important in dictating microglial responses. In support of this, Sayed and colleagues reported that partial TREM2 expression ($Trem2^{+/-}$) impaired microglia's response to localize around a laser-induced tissue injury and was associated with increased tau pathology compared with complete TREM2 absence ($Trem2^{-/-}$) in mutant

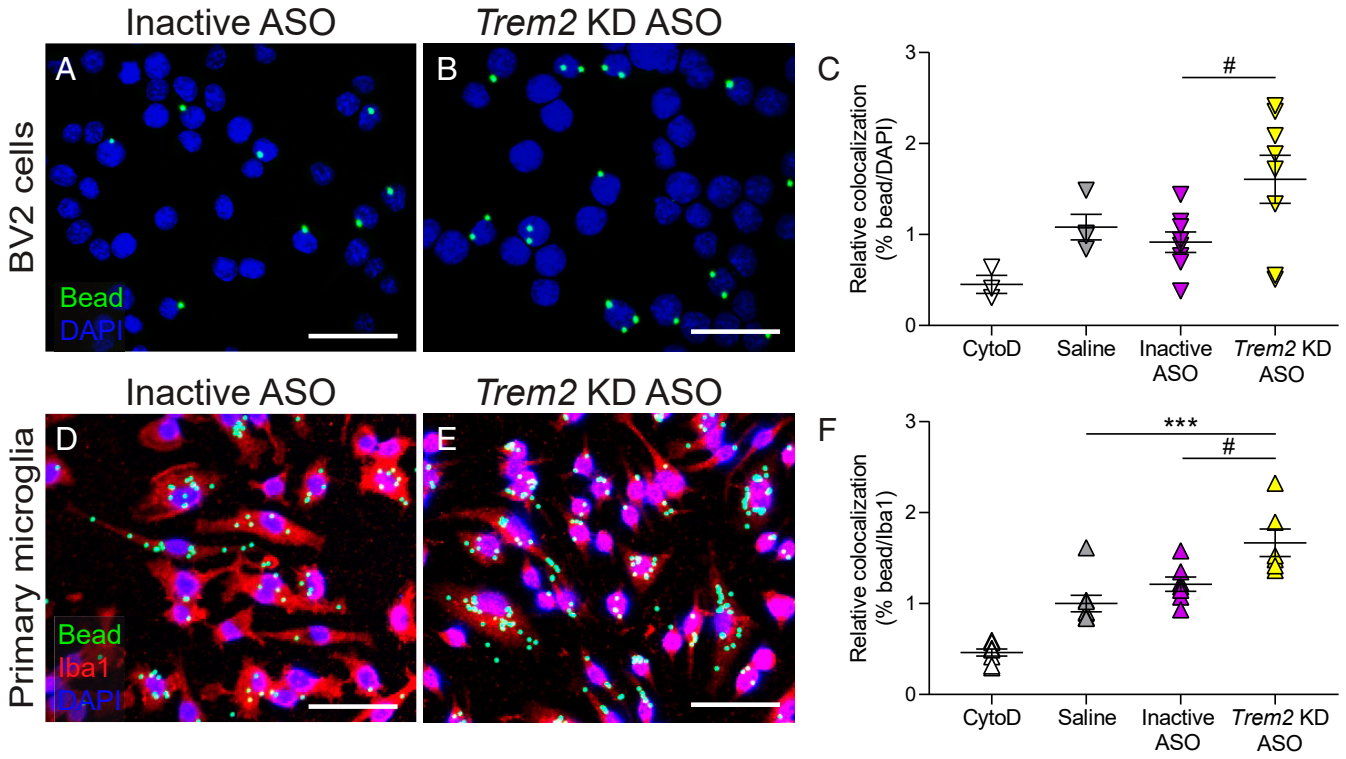

Fig. 6. ASO-mediated *Trem2* reduction increases phagocytosis in cultured cells. Phagocytosis of fluorescently labeled beads was measured in (*A*–*C*) BV2 cells and (*D*–*F*) primary nontransgenic mouse microglia following treatment with saline, inactive ASO, or *Trem2* KD ASO. Cytochalasin D (CytoD), an inhibitor of actin polymerization, was included as a control. Representative images are shown at 60× (BV2) or 20× (primary microglia). (Scale bar, 50 μM.) The percentage of bead colocalization with DAPI-positive cells (*C*) or with Iba1-positive cells (*F*) was quantified and shown as mean ± SEM relative to saline treatment. Triangles/circles represent individual wells (n = 4 to 8 wells/treatment in BV2 cells; n = 6 to 8 wells/treatment in primary microglia). One-way ANOVA with Tukey's multiple comparison test; $^{***}P < 0.001$ versus saline, $^{\#}P < 0.05$ versus inactive ASO.

P301S mice (26). *Trem2* reduction by ASO in our studies may achieve a level or function of TREM2 unlike loss-of-function variants; however, the level or persistence of TREM2 expression appears to be highly regulated and warrants further investigation. Similarly, temporary ASO-mediated *Trem2* reduction does not recapitulate models of TREM2 loss from birth, but it may avoid potential compensatory effects or other confounds associated with genetic knockout mouse models and may help evaluate the effects of varying TREM2 expression over time.

A consistent finding across many studies, including the present one, has been the lack of microglial clustering around plaques in the absence of TREM2. Previous data suggest this loss of microglial association imposes detrimental outcomes including increased plaque number (15) and neuritic dystrophy (16) and promotes a favorable environment for phosphorylated tau accumulation (19). Acute ASO-mediated *Trem2* reduction resulted in less microglia association with plaques coincident with less plaque load, thereby dissociating plaque-associated microglia from plaque pathogenesis. Alternatively, microglial responses, including clustering, may be elevated after *Trem2* reduction but then diminish over time as plaque load and/or proinflammatory signals decrease. Therefore, microglial activation may both mediate and be responsive to plaque deposition in a temporal manner. In the presence of plaques, microglia may acutely alter their inflammatory state to phagocytose and clear plaques, and once the plaques have been eliminated, microglia return to a more homeostatic state. In support of this hypothesis, we find that inflammatory gene expression is acutely increased 1 wk following *Trem2* lowering, prior to the clearance of plaques. At 1 mo following *Trem2* lowering, now with plaques reduced, inflammatory gene expression and microglial-plaque associations are dampened, suggesting that the microglia have returned to a less-activated state. Future studies may interrogate additional time points between 1 wk and 1 mo post-ASO injection to better understand this time course.

Based on previous data, the role for TREM2 in AD pathology may also be dependent on parallel disease pathologies. The APP/PS1 mice used in this study do not exhibit overt tau pathology or neurodegeneration, requiring other models to understand these aspects of human AD. However, we were able to detect increased phosphorylated tau in aged APP/PS1 mice that was significantly reduced with *Trem2*-lowering ASO treatment. The phosphorylated tau staining appeared plaque-like, perhaps indicative of dystrophic neurites. Although this phosphorylated tau may not be reminiscent of tau aggregates or neurofibrillary tangles evident in AD, it may represent a pathological cascade initiated by amyloid beta that was blunted by *Trem2* reduction. In models of pure tauopathy, *Trem2* deficiency mitigated tau-mediated cortical neurodegeneration and astrogliosis (28) but increased amyloid-induced tau spreading (19), suggesting TREM2 functions to promote pathology in the presence of tau alone or during later neurodegeneration phases of AD. In addition, expression of the R47H variant of TREM2 in PS19 mice attenuated tau pathology, neurodegeneration, and synapse loss (27). In line with our interpretation of ASO-mediated *Trem2* lowering effects on plaque pathology, these studies underscore a potential therapeutic window for TREM2 intervention whereby TREM2 deficiency during early plaque development may be damaging but during later tau deposition may be beneficial. Therefore, strategies aimed to target TREM2 at specific timepoints in disease may be effective toward mitigating both amyloid and tau pathologies.

Further TREM2-targeted studies will be needed to guide treatment strategies based on disease insult and progression.

Materials and Methods

APP/PS1 Transgenic Mice. APP/PS1 mice were purchased (Jackson Laboratories) and bred with B6C3 mice to obtain transgenic and nontransgenic littermates for experimental procedures. APP/PS1 mice (50) express a chimeric humanized amyloid precursor protein (Mo/HuAPP695) containing the Swedish (K595N/M596L) mutation and the mutant human presenilin 1 (PS1) lacking exon 9 (deltaE9), driven by the prion protein promoter. The APP/PS1 transgene was identified by PCR amplification of tail DNA using primers against the PS1 gene (5′-AAT AGA GAA CGG CAG GAG CAT CC-3′ and 5′-GCC ATG AGG GCA CTA ATC AT-3′). APP/PS1 mice exhibit notable differences in amyloid pathology between sexes, with females showing earlier and greater Aβ plaque deposition compared with male mice (51); therefore, experimental studies were restricted to male APP/PS1 mice. All mice were randomized across treatments by litter and date of birth.

Mice were housed at Washington University in St. Louis School of Medicine facilities under a controlled 12:12 h light:dark photoperiod with food and water ad libitum. All husbandry, surgical, and euthanasia procedures were approved by and performed according to regulations set by the Washington University Institutional Animal Care and Use Committee in accordance with federal standards. Actions to minimize animal discomfort, distress, pain, and injury were implemented to avoid unnecessary and unexpected complications due to treatment procedures.

ASOs. *Trem2*-lowering ASOs were designed with a phosphorothioate backbone consisting of 10 unmodified central nucleotides flanked on each end by 5 2′-*O*-methoxyethyl-modified nucleotides. This "gapmer" design allows for the recruitment of the enzyme RNaseH and degradation of *Trem2* mRNA while maintaining stability and tolerability in biological systems (52). An inactive ASO with identical backbone structure and sugar modifications but without an in vivo mRNA target was used in all experiments to account of any potential toxicity associated with the ASO.

ASOs were designed, screened in vitro, and provided for use by Ionis Pharmaceuticals (Carlsbad). ASOs sequences are as follows: *Trem2*-lowering ASO, 5′-ATGGAGTGTATCCCCGACGC-3′ and inactive ASO, 5′-CCTATAGGACTA-TCCAGGAA -3′. Predicted off-targets were determined by Basic Local Alignment Search Tool (blastn) analysis (https://blast.ncbi.nlm.nih.gov/), confirming the *Trem2*-lowering ASO does not bind any other transcript or genomic RNAs with full complementarity. Sequences with potential overlap (i.e., greater than 65% alignment at 100% identity and expect [E] values less than 30) were measured in tissues by real-time qPCR to exclude potential off-target effects.

Intracerebroventricular Injection of ASOs. *Trem2*-lowering and inactive ASOs were diluted in sterile saline and administered via intracerebroventricular (ICV) injection at a dose of 400 μg (in 10 μL) as previously described (53). In brief, mice were anesthetized by continuous isoflurane inhalation and positioned into a stereotaxic apparatus (Kopf). The skull was exposed and a 22-gauge needle with Hamilton syringe was positioned to −1.0 mm lateral (right hemisphere), 0.3 mm anterior, and 3.0 mm ventral relative to bregma (54). Following the single injection, the needle was withdrawn. The incision was sutured, and the mouse was placed on a heated recovery pad until ambulation. Nontransgenic mice received inactive ASO injections to account for potential surgical effects, and a separate cohort of untreated APP/PS1 mice euthanized at 10 mo of age was included in select analyses as an additional control. All surgical procedures, including aseptic technique and postoperative care, were performed in compliance with Washington University Institutional Animal Care and Use Committee policies and recommendations.

Euthanasia and Tissue Dissection. Following ASO treatment, mice were euthanized by transcardial perfusion with 0.03% heparinized phosphate buffered saline (PBS). Brains were immediately removed and separated into right (ipsilateral to ASO injection) and left hemispheres for tissue collection. Right hemispheres were further dissected into regions—frontal, parietal, occipital, and cerebellum—and snap frozen in liquid nitrogen. Left hemispheres were drop fixed in 4% paraformaldehyde for 24 h, placed into 30% sucrose solution for cryoprotection (at least 24 h), and frozen in cold (−25 to −35 °C) isopentane. Peripheral tissues including the spleen, liver, kidney, heart, and bone marrow were extracted postperfusion from select mice and snap frozen in liquid nitrogen. Frozen tissues were stored at −80 °C until additional processing.

mRNA Isolation and Real-Time qPCR Analysis. Brain tissue designated for real-time qPCR analysis was homogenized and RNA isolated using an RNeasy Mini Kit (Qiagen) per manufacturer protocol. RNA (20 ng/μL) samples, in duplicate, were probed for target genes using Taqman EXPRESS One-Step SuperScript qRT-PCR Universal kit (ThermoFisher Scientific) on an Applied Biosystems 7500 Fast Real-Time PCR system with 7500 Software version (v) 2.3. Quantitation of target genes was determined by comparative C_T ($\Delta\Delta C_T$) method, normalizing to *GAPDH* as an endogenous control. Taqman Gene Expression Assay (ThermoFisher Scientific), predesigned PrimeTime qPCR Primer Assays (Integrated DNA Technologies), or separate primer/probe sequences (Integrated DNA Technologies) were used to detect mRNA targets (*SI Appendix*, Table S1).

Immunohistochemistry. Fixed, frozen left hemisphere (contralateral to ASO injection) brain tissue designated for histology was cut on an HM 430 sliding microtome (ThermoFisher Scientific) into 50-μm sections and stored free floating at −20 °C in cryoprotectant solution (30 mM phosphate buffer, 30% ethylene glycol, 30% weight[wt]/volume [vol] sucrose) until use. Immunohistochemistry for TREM2, TREM2 with microglia (Iba1), amyloid beta (HJ3.4-biotin), amyloid beta (HJ3.4) with microglia (Iba1), and phosphorylated tau (AT8) are described in *SI Appendix*, *Supplementary Methods*.

HJ3.4B Plaque and AT8 Quantification. Immunohistochemical images were captured at 20× on the Hamamatsu NanoZoomer HT model whole slide imaging system (Hamamatsu Photonics) and exported using the NDP.view imaging software. The area of plaque deposition (HJ3.4-biotin) or phosphorylated tau (AT8) was obtained via ImageJ (NIH) by outlining the region of interest (ROI) and setting a minimum threshold level. An average of six sections for cortical plaque deposition (bregma −0.7 to −4.6 mm) and four sections for hippocampal deposition (bregma −1.6 to −4.6 mm) were measured per animal. Analyses were performed in a blinded fashion.

X-34 Staining and Quantification. Free-floating serial sections were washed in 1× PBS before incubating in 10 μM X-34 dissolved in 40% ethanol in 1× PBS (pH 10) for 20 min. Sections were then washed five times in 0.2% (wt/vol) NaOH in 80% ethanol for 2 min each, once in tap water for 10 min, and finally three times in 1× PBS for 5 min each. Tissue was mounted onto slides, and the coverslip sealed with Fluoromount-G.

X-34-stained tissue was imaged on a Zeiss Axioscan slide scanner (Zeiss) with a 10×/0.45 numerical aperture (NA) objective and 650 × 650 nm voxel size. All image acquisition and analysis settings were kept consistent between conditions. Analyses were performed in a blinded fashion using an average of six serial sections per animal between bregma 0.7 to −4.6 mm. Raw images were converted to TIFFs using Zen Blue (v. 2.6, Zeiss). Quantification of X-34–positive staining was performed by first creating ROI masks for cortical and hippocampal regions in ImageJ. The ROI masks and X-34 images were opened in Python (Python Software Foundation), and the pixels within the ROIs were analyzed to automatically identify X-34–positive signal above background. The number of X-34–positive pixels was then normalized to the size of the ROI to calculate the percentage of X-34–positive area. Representative images were obtained on a Nikon A1Rsi confocal microscope (Nikon Instruments Inc.) at 10× magnification.

Plaque and Microglial Image Analysis. Immunofluorescent images were captured on a Zeiss Axioscan slide scanner (Zeiss) with a 10×/0.45 NA objective and 650 × 650 nm voxel size. All image acquisition and analysis settings were kept consistent between conditions. Analyses were performed in a blinded fashion using three to four serial sections per animal between bregma −1.28 and −2.92 mm. Raw images were converted to TIFFs using Zen Blue (v. 2.6, Zeiss). A precise binary mask outlining the hippocampus was manually created for each image in ImageJ. Quantification of plaque areas and microglial density is described in *SI Appendix*, *Supplementary Methods*.

BV2 and Primary Microglia Cell Culture. BV2 cells (purchased from commercial vendor) were cultured in RPMI media supplemented with 10% fetal bovine serum (FBS) and 1% penicillin/streptomycin and plated at seeding density for ASO treatment. The following day, cells were treated with saline or 10 μM inactive ASO or *Trem2*-lowering ASO for 48 h. Primary microglia were isolated using previously published methods (55) with modification. Briefly, primary cortical glial cultures were generated from nontransgenic (B6C3 background) postnatal day 2 mouse pups and cultured in Dulbecco's Modified Eagle Media with 10% FBS and 1% penicillin/streptomycin. After the third day of culture, media supplemented with 10% L929 media was added to promote microglial homeostasis and subsequently changed every 3 d. The mixed glial cultures were grown for 10 d until confluency. Microglia were

purified by agitation on an orbital shaker at 270 rpm for 2 h at 37 °C, centrifuged at 300 × *g* for 5 min, and plated onto Falcon 8-well chambered cell culture slides (ThermoFisher Scientific) coated with 100 μg/mL poly-D-lysine. Microglia were maintained in culture for two days prior to treatment with saline or 10 μM of inactive ASO or *Trem2*-lowering ASO for 96 h, with ASO-containing media being replaced after 48 h.

In Vitro Phagocytosis Assay. Following ASO treatments, BV2 cells and primary microglia were assayed for phagocytosis activity. At 1 h prior to the phagocytosis measurements, 10 μM cytochalasin D (Sigma Aldrich) was added to select wells as a negative control. Fluoresbrite YG Microspheres (Polysciences) were diluted 1:1,000 in media and allowed to incubate on the cells at 37 °C for 2 h. The media was then removed, and the cells were washed three times with 1× PBS. Cells were fixed with ice-cold methanol at 4 °C for 15 min followed by 1× PBS washes. BV2 cells were stained with DAPI (1:1,000). Primary microglia were labeled with Iba1 primary antibody (1:1,000, Wako Chemicals) diluted in 0.1% bovine serum albumin (BSA)/PBS overnight followed by incubation in secondary antibody (anti-rabbit AlexaFluor 594, 1:500; ThermoFisher Scientific) and DAPI staining (1:1,000). Images ($n = 5$ images/well; 3 wells for cytochalasin D treatment, 4 to 8 wells for saline and ASO treatment) were captured at 20× on a Nikon A1Rsi confocal microscope and blinded for analysis. Bead colocalization with DAPI (BV2 cells) or Iba1 (primary microglia) was quantified by ImageJ colocalization plugin and threshold-based cell count (DAPI).

Statistical Analyses. Data were graphed as mean ± SEM and analyzed using GraphPad Prism 8 software (GraphPad Software). mRNA levels for all tested genes were expressed relative to nontransgenic or saline/inactive ASO controls and evaluated by one-way ANOVA Tukey's multiple comparison post hoc analysis. At least 20% *Trem2* KD by mRNA analysis was deemed a successful treatment; mice failing to reach this prerequisite ($n = 1$) were excluded from all subsequent analysis. Quantification of the amyloid beta plaque and phosphorylated tau area, total microglia, and in vitro phagocytosis were compared using one-way ANOVA with Tukey's multiple comparison post hoc test. Microglial coverage of plaques was analyzed using an unpaired *t* test. A value of $P < 0.05$ was deemed significant for all analyses.

Data Availability. All study data are included in the article and/or *SI Appendix*.

ACKNOWLEDGMENTS. Support for this work was provided by the BrightFocus Foundation (T.M.M.), a Pilot Project Award from the Hope Center for Neurological Disorders at Washington University in St. Louis (T.M.M.), and National Institute of Neurological Disorders and Stroke R01NS078398 (T.M.M.). Wide-field and confocal image acquisition were performed in part through the use of the Washington University Center for Cellular Imaging (WUCCI) supported by the Washington University School of Medicine, The Children's Discovery Institute of Washington University, St. Louis Children's Hospital (CDI-CORE-2015-505 and CDI-CORE-2019-813), and the Foundation for Barnes-Jewish Hospital (3770 and 4642). Additional microscopy work was supported by the Hope Center Alafi Neuroimaging Laboratory and an NIH Shared Instrumentation Grant award to Washington University (S10 RR027552). We thank Nathan Pomper for his technical contributions pertaining to *Trem2* immunostaining and Alex Cammack, Ph.D., for his thorough review and critique of the project and manuscript.

1. R. J. Bateman *et al.*; Dominantly Inherited Alzheimer Network, Clinical and biomarker changes in dominantly inherited Alzheimer's disease. *N. Engl. J. Med.* **367**, 795–804 (2012).
2. C. R. Jack Jr *et al.*, Tracking pathophysiological processes in Alzheimer's disease: An updated hypothetical model of dynamic biomarkers. *Lancet Neurol.* **12**, 207–216 (2013).
3. V. Calsolaro, P. Edison, Neuroinflammation in Alzheimer's disease: Current evidence and future directions. *Alzheimers Dement.* **12**, 719–732 (2016).
4. R. Ismail *et al.*, The relationships between neuroinflammation, beta-amyloid and tau deposition in Alzheimer's disease: A longitudinal PET study. *J. Neuroinflammation* **17**, 151 (2020).
5. J. W. Kinney *et al.*, Inflammation as a central mechanism in Alzheimer's disease. *Alzheimers Dement. (N. Y.)* **4**, 575–590 (2018).
6. J. Verheijen, K. Sleegers, Understanding Alzheimer disease at the interface between genetics and transcriptomics. *Trends Genet.* **34**, 434–447 (2018).
7. R. Guerreiro *et al.*; Alzheimer Genetic Analysis Group, TREM2 variants in Alzheimer's disease. *N. Engl. J. Med.* **368**, 117–127 (2013).
8. T. Jonsson *et al.*, Variant of TREM2 associated with the risk of Alzheimer's disease. *N. Engl. J. Med.* **368**, 107–116 (2013).
9. I. R. Turnbull *et al.*, Cutting edge: TREM-2 attenuates macrophage activation. *J. Immunol.* **177**, 3520–3524 (2006).
10. A. Deczkowska, A. Weiner, I. Amit, The physiology, pathology, and potential therapeutic applications of the TREM2 signaling pathway. *Cell* **181**, 1207–1217 (2020).
11. H. Keren-Shaul *et al.*, A unique microglia type associated with restricting development of Alzheimer's disease. *Cell* **169**, 1276–1290.e17 (2017).
12. S. Krasemann *et al.*, The TREM2-APOE pathway drives the transcriptional phenotype of dysfunctional microglia in neurodegenerative diseases. *Immunity* **47**, 566–581.e9 (2017).
13. T. R. Jay *et al.*, TREM2 deficiency eliminates TREM2+ inflammatory macrophages and ameliorates pathology in Alzheimer's disease mouse models. *J. Exp. Med.* **212**, 287–295 (2015).
14. J. D. Ulrich *et al.*, Altered microglial response to Aβ plaques in APPPS1-21 mice heterozygous for TREM2. *Mol. Neurodegener.* **9**, 20 (2014).
15. Y. Wang *et al.*, TREM2 lipid sensing sustains the microglial response in an Alzheimer's disease model. *Cell* **160**, 1061–1071 (2015).
16. P. Yuan *et al.*, TREM2 haplodeficiency in mice and humans impairs the microglia barrier function leading to decreased amyloid compaction and severe axonal dystrophy. *Neuron* **92**, 252–264 (2016).
17. C. Condello, P. Yuan, A. Schain, J. Grutzendler, Microglia constitute a barrier that prevents neurotoxic protofibrillar Aβ42 hotspots around plaques. *Nat. Commun.* **6**, 6176 (2015).
18. Y. Wang *et al.*, TREM2-mediated early microglial response limits diffusion and toxicity of amyloid plaques. *J. Exp. Med.* **213**, 667–675 (2016).
19. C. E. G. Leyns *et al.*, TREM2 function impedes tau seeding in neuritic plaques. *Nat. Neurosci.* **22**, 1217–1222 (2019).
20. T. R. Jay *et al.*, Disease progression-dependent effects of TREM2 deficiency in a mouse model of Alzheimer's disease. *J. Neurosci.* **37**, 637–647 (2017).
21. S. Parhizkar *et al.*, Loss of TREM2 function increases amyloid seeding but reduces plaque-associated ApoE. *Nat. Neurosci.* **22**, 191–204 (2019).
22. L. Sheng *et al.*, Microglial Trem2 induces synaptic impairment at early stage and prevents amyloidosis at late stage in APP/PS1 mice. *FASEB J.* **33**, 10425–10442 (2019).
23. M. Kawabori *et al.*, Triggering receptor expressed on myeloid cells 2 (TREM2) deficiency attenuates phagocytic activities of microglia and exacerbates ischemic damage in experimental stroke. *J. Neurosci.* **35**, 3384–3396 (2015).
24. M. Saber, O. Kokiko-Cochran, S. S. Puntambekar, J. D. Lathia, B. T. Lamb, Triggering receptor expressed on myeloid cells 2 deficiency alters acute macrophage distribution and improves recovery after traumatic brain injury. *J. Neurotrauma* **34**, 423–435 (2017).
25. C. Cantoni *et al.*, TREM2 regulates microglial cell activation in response to demyelination in vivo. *Acta Neuropathol.* **129**, 429–447 (2015).
26. F. A. Sayed *et al.*, Differential effects of partial and complete loss of TREM2 on microglial injury response and tauopathy. *Proc. Natl. Acad. Sci. U.S.A.* **115**, 10172–10177 (2018).
27. M. Gratuze *et al.*, Impact of TREM2R47H variant on tau pathology-induced gliosis and neurodegeneration. *J. Clin. Invest.* **130**, 4954–4968 (2020).
28. C. E. G. Leyns *et al.*, TREM2 deficiency attenuates neuroinflammation and protects against neurodegeneration in a mouse model of tauopathy. *Proc. Natl. Acad. Sci. U.S.A.* **114**, 11524–11529 (2017).
29. S. M. Bemiller *et al.*, TREM2 deficiency exacerbates tau pathology through dysregulated kinase signaling in a mouse model of tauopathy. *Mol. Neurodegener.* **12**, 74 (2017).
30. M. Garcia-Alloza *et al.*, Characterization of amyloid deposition in the APPswe/PS1dE9 mouse model of Alzheimer disease. *Neurobiol. Dis.* **24**, 516–524 (2006).
31. J. L. Jankowsky *et al.*, Mutant presenilins specifically elevate the levels of the 42 residue beta-amyloid peptide in vivo: Evidence for augmentation of a 42-specific gamma secretase. *Hum. Mol. Genet.* **13**, 159–170 (2004).
32. W. Kamphuis *et al.*, GFAP isoforms in adult mouse brain with a focus on neurogenic astrocytes and reactive astrogliosis in mouse models of Alzheimer disease. *PLoS One* **7**, e42823 (2012).
33. A. A. Raha *et al.*, Neuroprotective effect of TREM-2 in aging and Alzheimer's disease model. *J. Alzheimers Dis.* **55**, 199–217 (2017).
34. M. Matarin *et al.*, A genome-wide gene-expression analysis and database in transgenic mice during development of amyloid or tau pathology. *Cell Rep.* **10**, 633–644 (2015).
35. L. F. Lue *et al.*, TREM2 protein expression changes correlate with Alzheimer's disease neurodegenerative pathologies in post-mortem temporal cortices. *Brain Pathol.* **25**, 469–480 (2015).
36. S. E. Perez *et al.*, Neocortical and hippocampal TREM2 protein levels during the progression of Alzheimer's disease. *Neurobiol. Aging* **54**, 133–143 (2017).
37. L. Ma *et al.*, Expression and processing analyses of wild type and p.R47H TREM2 variant in Alzheimer's disease brains. *Mol. Neurodegener.* **11**, 72 (2016).
38. Y. Zhao *et al.*, TREM2 is a receptor for β-amyloid that mediates microglial function. *Neuron* **97**, 1023–1031.e7 (2018).
39. M. A. Kurt, D. C. Davies, M. Kidd, K. Duff, D. R. Howlett, Hyperphosphorylated tau and paired helical filament-like structures in the brains of mice carrying mutant amyloid precursor protein and mutant presenilin-1 transgenes. *Neurobiol. Dis.* **14**, 89–97 (2003).
40. M. Pérez, M. A. Morán, I. Ferrer, J. Avila, P. Gómez-Ramos, Phosphorylated tau in neuritic plaques of APP(sw)/Tau (vlw) transgenic mice and Alzheimer disease. *Acta Neuropathol.* **116**, 409–418 (2008).
41. J. Shin, S. Park, H. Lee, Y. Kim, Thioflavin-positive tau aggregates complicating quantification of amyloid plaques in the brain of 5XFAD transgenic mouse model. *Sci. Rep.* **11**, 1617 (2021).

42. W. J. Meilandt *et al*., Trem2 deletion reduces late-stage amyloid plaque accumulation, elevates the Aβ42:Aβ40 ratio, and exacerbates axonal dystrophy and dendritic spine loss in the PS2APP Alzheimer's mouse model. *J. Neurosci.* **40**, 1956–1974 (2020).
43. K. I. Mosher, T. Wyss-Coray, Microglial dysfunction in brain aging and Alzheimer's disease. *Biochem. Pharmacol.* **88**, 594–604 (2014).
44. K. Schlepckow *et al*., Enhancing protective microglial activities with a dual function TREM2 antibody to the stalk region. *EMBO Mol. Med.* **12**, e11227 (2020).
45. S. Wang *et al*., Anti-human TREM2 induces microglia proliferation and reduces pathology in an Alzheimer's disease model. *J. Exp. Med.* **217**, e20200785 (2020).
46. S. S. Kang *et al*., Microglial translational profiling reveals a convergent APOE pathway from aging, amyloid, and tau. *J. Exp. Med.* **215**, 2235–2245 (2018).
47. H. B. Dean, E. D. Roberson, Y. Song, Neurodegenerative disease-associated variants in TREM2 destabilize the apical ligand-binding region of the immunoglobulin domain. *Front. Neurol.* **10**, 1252 (2019).
48. D. L. Kober *et al*., Neurodegenerative disease mutations in TREM2 reveal a functional surface and distinct loss-of-function mechanisms. *eLife* **5**, e20391 (2016).
49. W. Song *et al*., Alzheimer's disease-associated TREM2 variants exhibit either decreased or increased ligand-dependent activation. *Alzheimers Dement.* **13**, 381–387 (2017).
50. J. L. Jankowsky *et al*., Co-expression of multiple transgenes in mouse CNS: A comparison of strategies. *Biomol. Eng.* **17**, 157–165 (2001).
51. J. Wang, H. Tanila, J. Puoliväli, I. Kadish, T. van Groen, Gender differences in the amount and deposition of amyloidbeta in APPswe and PS1 double transgenic mice. *Neurobiol. Dis.* **14**, 318–327 (2003).
52. T. C. Roberts, R. Langer, M. J. A. Wood, Advances in oligonucleotide drug delivery. *Nat. Rev. Drug Discov.* **19**, 673–694 (2020).
53. S. L. DeVos, T. M. Miller, Direct intraventricular delivery of drugs to the rodent central nervous system. *J. Vis. Exp.* e50326 (2013).
54. K. B. J. Franklin, G. Paxinos, *Paxinos and Franklin's The Mouse Brain in Stereotaxic Coordinates* (Academic Press, an imprint of Elsevier, Amsterdam, ed. 4, 2013), pp. 1–360.
55. S. Schildge, C. Bohrer, K. Beck, C. Schachtrup, Isolation and culture of mouse cortical astrocytes. *J. Vis. Exp.* 50079 10.3791/50079 (2013).